Diffusion and Orientability of Rigid-Rodlike Molecules in Solution

Jeffrey A. Odell, Andrew Keller,* and Edward D. T. Atkins

H. H. Wills Physics Laboratory, University of Bristol, Bristol BS8 1TL, United Kingdom.
Received August 27, 1984

ABSTRACT: Dilute and semidilute solutions of poly(*p*-phenylenebenzbisthiazole) (PBT) have been subjected to the elongational flow field created by a Taylor four-roll mill, yielding significant new information on the orientability and diffusion of this near-ideal rigid-rod molecule. The results show that for sufficiently long residence times in the elongational flow field PBT exhibits a transition between isotropic solution and liquid-crystal-like behavior at low concentrations. The rotational diffusion coefficient ($\tilde{D}_r$) is found to increase with orientation, in qualitative agreement with existing theories which incorporate mean constraints for rod–rod interaction. However, the measured value of $\tilde{D}_r$ is >3 orders of magnitude higher than that predicted by these theories, pointing to much lower interference between neighboring rods than had been previously assumed. Modifications to these assumptions are proposed which relax mutual interference constraints and yield good agreement with the measured value of $\tilde{D}_r$. In spite of this fit computer simulations indicate that the rods will tend to escape through instantaneous gaps opening up statistically, rather than be contained by any mean constraint. This calls for an altogether different basis for the interpretation of the interaction between rodlike molecules than is presently provided by mean value theories.

1. Introduction

The work presented here is a study of the response of rigid-rod molecules to the orienting influence of a pure elongational flow field. The initial direction of the work was to explore the enhancement of liquid-crystal formation which is anticipated to arise from such flow fields. This subject will indeed be touched upon; nevertheless the main part of the work became concerned with the primary mechanisms of orientation and diffusion of entangled rodlike molecules after it was realized that our experiments offered a fruitful approach to this fundamental issue. Such mechanisms are central to the behavior of rigid-rod molecules as well as to the processing and orientability of such materials and are a precondition for liquid-crystal formation when this takes place. A preliminary note of our results has already been published.[1] The present contribution represents the full work underlying that note.

The material of our investigation is poly(*p*-phenylenebenzbisthiazole) (PBT), a member of a new class of aromatic heterocyclic polymers possessing extremely rigid backbone chains. The chemical structure of PBT is shown in Figure 1. Such polymers form liquid-crystal-like solutions in strong-acid solvents. The rheology of such solutions has been extensively investigated.[2-4] The polymers can be processed from the nematic phase into fibers and films of exceptional stiffness and strength, together with great thermal stability.[5] The structure of oriented fibers and films of PBT has been the subject of much previous work.[6-9]

The PBT molecule itself has been shown to be among the most rigid and linear in this class and, for most purposes, can be regarded as an ideal perfectly rigid-rodlike molecule.[10] For this reason PBT makes an excellent model system for the examination of processes of orientation and diffusion of rodlike molecules in solution.

A recent important theory by Doi[11] and Doi and Edwards[12,13] provides the framework for an understanding of the behavior of such systems for the concentration range in which the molecules are strongly entangled, but where volume exclusion effects are still relatively unimportant. This concentration domain can be expressed by

$$1/dL^2 \gg c \gg 1/L^3$$

where c is the number of molecules per unit volume, L is the length of the molecules, and d is the molecular diameter.

The rotational diffusion coefficient ($\tilde{D}_r$) of the rigid rods in an entangled strongly interacting system is a parameter that describes molecular motion, the perfection of orientation in flowing solutions, and the consequent macroscopic time constant of relaxation, τ_c, where by ref 14

$$\tau_c \approx \tfrac{1}{6}\tilde{D}_r$$

$\tilde{D}_r$ itself is expected to be a strongly correlated function of solvent viscosity, concentration, molecular dimensions, and the state of orientation of the molecules.

For an isotropic solution the Doi–Edwards theory predicts

$$D_r \approx D_{r_0}/(cL^3)^2$$

where D_{r_0} is the unhindered rotational diffusion coefficient of the molecule at infinite dilution and D_r is the rotational diffusion coefficient of an entangled but isotropic solution. The theory calculates $\tilde{D}_r$ as a perturbation from the isotropic case and predicts an increasing value of $\tilde{D}_r$ with increasing orientation, qualitatively accounting for the nonlinear viscoelasticity usually observed in liquid-crystalline solutions in general.

Previous work in this laboratory has examined the response of flexible[15,16] and semiflexible[17] polymer molecules to well-defined elongational flow fields. In the course of this work we developed methods by which elongational flow fields could be created and the resulting orientations observed. One of these was the four-roll mill,[15,18,19] which generates an elongational flow field by pure shear in the form of "stretching" the fluid elements containing the polymer with one lateral direction held constant (Figure 2), corresponding to a pure elongational flow field with no rotational component. While the stretching force, the strain rate, is practically uniform throughout the interior of the mill, the fluid element resides for the longest time when passing through or near the center of the apparatus and thus will be most elongated along the outgoing axis (0–X in Figure 2). (The center of the apparatus, $Y = X = 0$ in Figure 2, is a stagnation point with infinite residence time.) With flexible molecules this had the consequence that molecular elongation (which was practically full-chain elongation) was localized as a thin sheet (as seen edgewise) along the 0–X line. As will be seen, with rigid molecules the orientation is not localized; nevertheless the 0–X line will appear to be the site of rather special events.

0024-9297/85/2218-1443$01.50/0

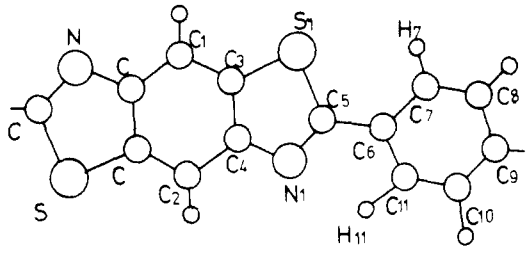

Figure 1. Repeating unit of poly(*p*-phenylenebenzbisthiazole) (PBT).

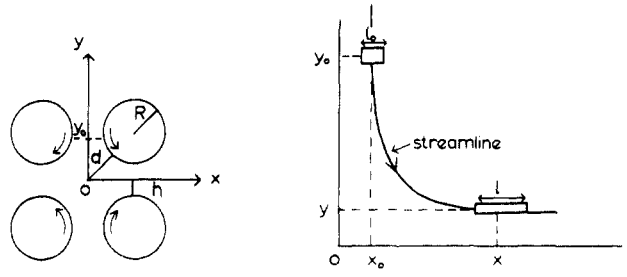

(a) (b)

Figure 2. (a) Schematic plan view of the four-roll mill. (b) Diagrammatic representation of the extension of a fluid element along an arbitrary stream line in the four-roll mill.

The time dependence of the orientational distribution function (ρ) for rigid-rod molecules in pure shear in the $X-Y$ plane (as in the four-roll mill) can be derived from

$$\frac{\partial \rho}{\partial t} = \dot{\epsilon}\left[\frac{\partial(\rho \sin 2\phi)}{\partial \phi} - \frac{1}{\sin\theta}\frac{\partial \theta}{\partial(\rho \sin^2\theta \cos\theta \cos 2\theta)}\right] + \tilde{D}_r\left[\frac{1}{\sin\theta}\frac{\partial \theta}{\partial\left(\sin\theta \dfrac{\partial \rho}{\partial \theta}\right)} + \frac{1}{\sin^2\theta}\frac{\partial^2 \rho}{\partial \phi^2}\right]$$

where θ is the angle with Z and ϕ is the angle with X projected onto the $X-Y$ plane. $\dot{\epsilon}$ is the strain rate.[20] The first term represents the response of the molecules to the flow field, and the second term the disorientational Brownian diffusion of molecules.

A series expansion of this formula coupled with the interpretation of ρ in terms of induced retardation (B)[21] leads to

$$\frac{B}{B_0} = \frac{2\dot{\epsilon}}{15\tilde{D}_r}(1 - e^{-6\tilde{D}_r t}) \qquad \text{for } \frac{\dot{\epsilon}}{\tilde{D}_r} \lesssim 1 \tag{1}$$

where B_0 is the maximum retardation (perfect orientation).

A recent work by Peterlin[22] leads to similar results as a first approximation for rigid spheroids in pure shear flow. The PBT molecule possesses extremely high intrinsic retardation, so that in the four-roll mill the orientation induced by the flow field and the disorientational diffusion processes can be well monitored by measuring the optical retardation. In principle, the examination of induced retardation in response to a static or changing flow field of known well-defined nature can enable the assessment of $\tilde{D}_r$ as a function of molecular orientation and solution concentration.

To a good approximation the almost uniform extensional flow field inside the four-roll mill can be quantitifed according to Torza[23] by

$$\dot{\epsilon} = \frac{2\omega}{\pi} \ln\left(\frac{R+h}{h}\right) \tag{2}$$

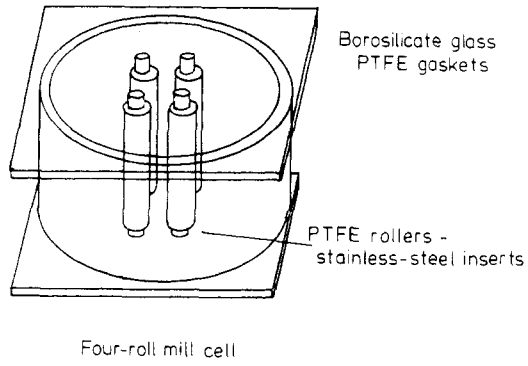

Four-roll mill cell

Figure 3. Four-roll mill cell built for PBT solutions.

where R is the roller radius, $2h$ is the roller separation, and ω is the angular velocity of the rollers (see Figure 2a).

As we shall see in ensuing sections, the four-roll mill apparatus can yield information about $\tilde{D}_r$ and its dependence on orientation by three distinct methods, all relying on observation within the same field of view between the rollers. The methods are outlined as follows:

(I) The induced retardation at the center of the mill corresponds to a balance of orientational effects of the flow field and disorientational effects of rotational diffusion, broadly determined by eq 1 in the long-term equilibrium limit.

(II) The entrance region of the four-roll mill (the nip region between the rollers on the incoming axis) yields information on the dynamic response of the molecules to a changing, but well-defined, flow field.

(III) The mill can be abruptly stopped and the decay of retardation from an oriented state, in the absence of an elongational flow field, yields the relaxation time of the molecules τ_c, which is related to $\tilde{D}_r$ by

$$\tau_c \approx 1/6\tilde{D}_r$$

2. Experimental Section

The polymer used in this study was synthesized by the Stanford Research Institute. It is characterized by an intrinsic viscosity of 32 dL/g. The rigorous exclusion of water during preparation of PBT solutions is essential, since the presence of water is known to cause molecular aggregation.[3] The polymer was dried under vacuum at 100 °C for 7 days. Solutions were prepared by magnetic stirring in sealed vessels with a solvent of 97.5% fresh methanesulfonic acid + 2.5% chlorosulfonic acid, which has the effect of scavenging residual water. Four concentrations have been used in this study: 0.025% (w/w), representing the lowest concentration that is presently practicable to run in the four-roll mill, 0.5% (w/w), representing the upper limit of the stated range of applicability of the Doi–Edwards theory, 0.75% (w/w), and 1% (w/w).

The first criterion to be met by the apparatus was to obviate, as far as possible, any corrosion inside the four-roll mill. This is important in the present case, since the evolution of even microscopic gas bubbles in the cell can make optical observations of low fields and molecular orientation impossible. This has been achieved by making all surfaces in the four-roll mill cell of poly(tetrafluoroethylene) (PTFE) or borosilicate glass. Both of these materials are found to be highly resistant to methanesulfonic acid and chlorosulfonic acid.

A diagram of the cell is shown in Figure 3. The containing vessel is made from 6-mm borosilicate float glass selected specially for its optical properties. The rollers are made of PTFE with totally enclosed stainless steel reinforcing pins. The cell is assembled with PTFE gaskets and an external stainless steel clamping arrangement.

A further requirement of the cell is that it be hermetically sealed, insofar as this is consistent with the provision of roller drive arrangements. This requirement is necessary to prevent the escape of highly corrosive (and toxic) acid vapors and to prevent the ingress of water vapor, which can rapidly coagulate

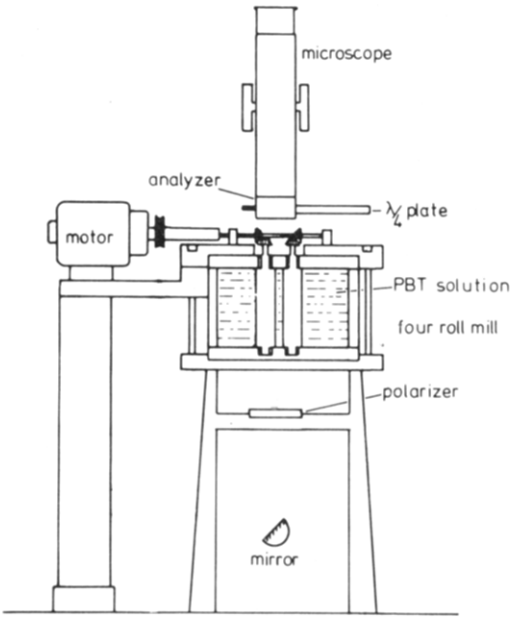

Figure 4. Optical arrangement for birefringence measurements.

PBT solutions, even in 1% proportions. This is achieved by the use of PTFE seals around the roller-bearing surfaces and PTFE plugs in the cell filling and cell vent holes.

The cell ancillary equipment, drive arrangements, and optical system are shown in Figure 4. A parallel beam of light from a laser, mercury, or tungsten halide lamp is directed vertically into the cell by means of a mirror mounted at 45°. A rotatable analyzer and polarizer are incorporated above and below the cell to enable birefringence observations and measurements between crossed polars.

3. Observations of Induced Orientation

3.1. Central Flow Field. Figure 5a shows the field of view for a low shear rate ($\sim 3\ s^{-1}$) with crossed polarizer and analyzer positioned at 45° to the mill inlet and outlet directions for a 0.5% (w/w) PBT solution. As predicted for these stiff linear polymers the effect of the elongational flow field (here realized by pure shear) is to produce a nonlocalized orientation in the flow field, observed as a uniformly bright field within the area enclosed by the rollers. With the polarizer and analyzer directions parallel and perpendicular to the entry and exit directions (0–Y and 0–X in Figure 2b) the same area becomes uniformly dark (Figure 5b). This indicates that the transmission axes of the birefringent solution coincide with these two directions. Insertion of a full-wave plate shows further that the molecules are aligned with their long axes toward the exit axis throughout the interior of the mill. Both the uniformity and the sign of the orientation are consistent with the pure elongational flow field, to be explained further below. Figure 5c shows the birefringent field viewed at a higher shear rate ($10\ s^{-1}$). In this case birefringent colors are observable as the retardation becomes greater than one wavelength of the tungsten halide light. It is interesting to note that the colors are not, contrary to prior expectation, entirely uniform across the mill but show concentric rings of varying retardation corresponding to a small decrease in retardation approaching the center of the mill and a corresponding increase toward the exit. Figure 5c is printed through a colored filter to enhance the contrast of the observed effect. A detailed examination of earlier papers shows that the effect of reducing birefringence in the center of the mill can be directly accounted for by a small reduction in shear rate, documented by Taylor in 1934,[18] although not specifically commented upon at the time.

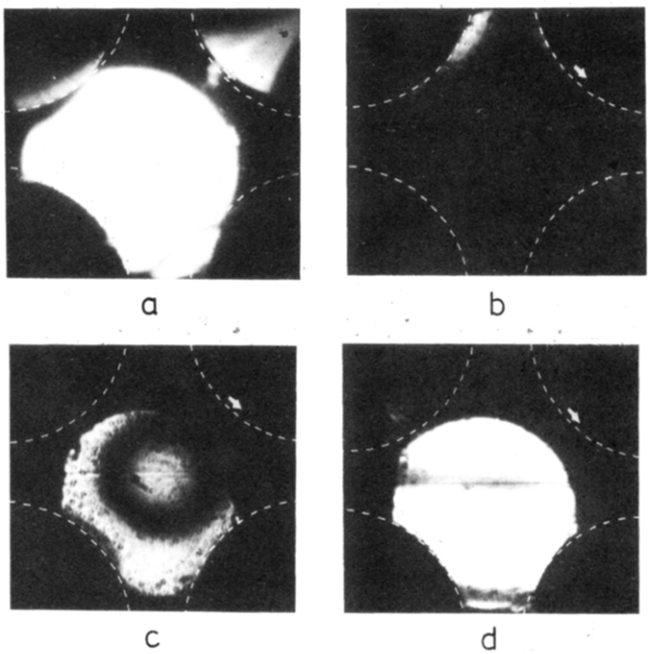

Figure 5. (a) Birefringence in the central flow field with crossed polars at 45° to the mill inlet and outlet directions ($\dot{\epsilon} = 3\ s^{-1}$). (b) With crossed polars at 90° to the inlet and outlet directions. (c) Birefringence at higher strain rates ($\dot{\epsilon} = 10\ s^{-1}$, polars at 45°). (d) Highly birefringent central band ($\dot{\epsilon} = 5\ s^{-1}$; polars at 45°).

In the present instance we are operating with a solution with a high rotational diffusion coefficient (of the order of $20\ s^{-1}$; see section 5.1). Through eq 1 this gives rise to a very short time constant $\tau_c = (1/6\bar{D}_r)$ of about 10 ms, so that the orientation of the molecules, and hence the observed birefringence, can respond almost instantly to changes in strain rate in the mill compared with the residence time along any stream line through the mill. This is the reason why the birefringence is not confined (i.e., localized) to stream lines that pass through the stagnation point, as in the case of flexible molecules which require a long residence time to achieve an oriented state.[15–19] The rapid response also explains why the retardation is found to decrease almost immediately in response to the slight nonuniformity of the central flow field. The small variation of the strain rate in the central flow field has not previously been recognized earlier because previous systems examined in the four-roll mill have had much longer time constants and so could not respond instantaneously to changes in the flow field.

3.2. Central Dark Band. An interesting departure from the uniform flow field is the observation of a highly localized dark band lying along the exit axis of the mill. Occasionally the band has been observed to have an overall higher birefringence than the rest of the field where the retardation (B) in the band shows up as colors ($B > \lambda$) against a light background ($B < \lambda$) (Figure 5d). This band is envisaged as the projection of a thin sheet extending down through the mill. It may always possess a higher birefringence than the rest of the flow field, but because of the difficulty of observing directly down a sheet ~ 50 μm thick and 2 cm deep, it is normally seen as a discontinuity in overall refractive index, i.e., a dark band. (We expect this thin sheet lying along the exit symmetry axis to be flexing slightly due to flow perturbations, so that during observations at grazing incidence the image and birefringence become somewhat confused.)

The origin of this band is at present still uncertain, but it most probably represents the liquid-crystalline state. The only property unique to the exit axis is that molecules

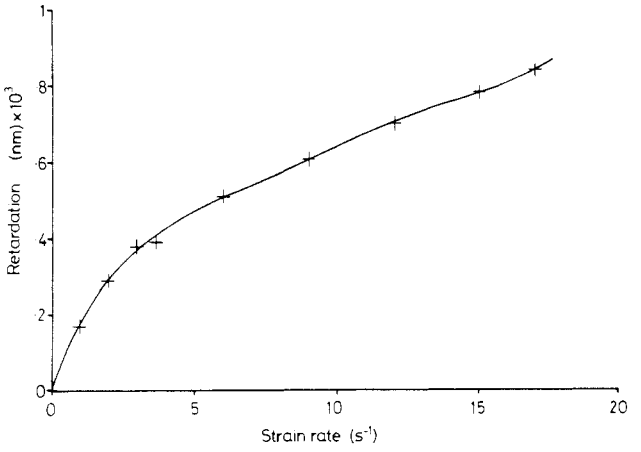

Figure 6. Retardation vs. strain rate in the center of the mill for 0.5% solution.

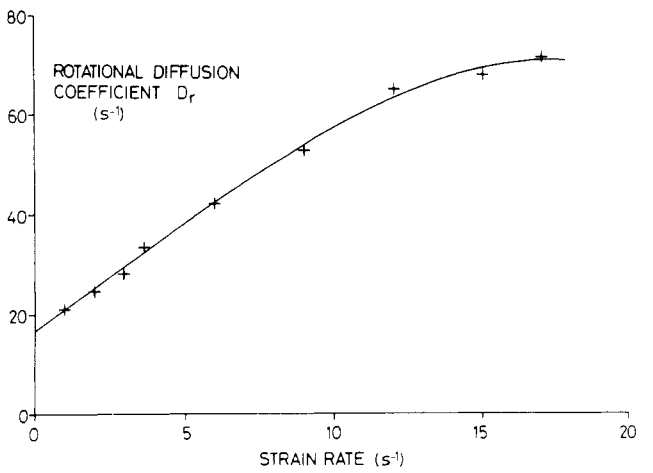

Figure 7. Rotational diffusion coefficient vs. strain rate.

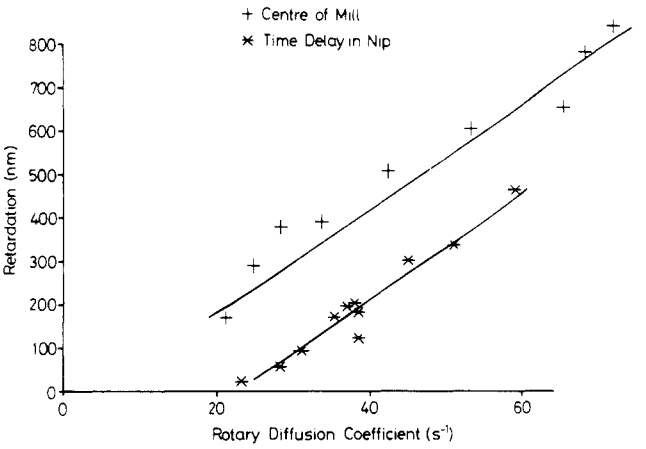

Figure 8. Variation of rotational diffusion coefficient with retardation from the center of the mill (equilibrium method) and the nip region (dynamic method).

passing along this axis go through a stagnation point (the center point (0)); hence they have a much longer residence time in the flow field than do molecules that pass along any other stream line. As stated earlier, $\tilde{D}_r$ is of the order of 20 s^{-1}, giving a τ_c time constant of about 10 ms, so that we would expect all time-dependent effects to have disappeared after about 100 ms, which is small compared with the residence time along any stream line through the mill. The phenomenon does however appear to have a certain generality since similar dark bands (though not explicitly of greater Δn) have been seen in poly(γ-benzyl L-glutamate) (PBLG) solutions, also well below liquid-crystal concentrations.

It is well-known that in a stationary system there is an isotropic solution → liquid crystal transformation on increase of concentration. It is anticipated that this transition will be promoted by orientational flow; i.e., a solution sufficiently dilute to be on the isotropic liquid side of the phase boundary could become liquid crystal through a displacement of the isotropic solution–liquid crystal coexistence curve to lower concentrations. It will be evident that the method offers a direct approach to this flow-promoted liquid-crystal formation. The reason why this effect should be localized in the four-roll mill is more likely the increased residence time along the exit axis allowing the phase transformation to proceed, rather than more pronounced chain orientation in itself.

4. Measurement of Rotational Diffusion Coefficients

4.1. Central Flow Field (Method I). In the central field of the four-roll mill the observed retardation is expected to be related to the maximum retardation as a function of strain rate $\dot{\epsilon}$ by eq 1. In the central region of the four-roll mill, where the strain rate is essentially constant for long residence times, the time-dependent term (in parentheses in eq 1) rapidly approaches unity, so that

$$B/B_0 = 2\dot{\epsilon}/15\tilde{D}_r \quad (3)$$

Given a knowledge of B_0, which we have deduced from direct measurements on oriented and extremely thin films, we can find $\tilde{D}_r$ as a function of strain rate and hence as a function of molecular orientation.

This is, of course, only the case when B is small; as B approaches its limiting value B_0 the relationship between B and $1/\tilde{D}_r$ (eq 3) becomes nonlinear. In the present case however, B/B_0 never exceeds 0.03.

As an illustration, Figure 6 shows the retardation measured in the center of the mill as a function of the applied strain rate for a 0.5% solution. The relationship is nonlinear, contrary to what would be expected from eq 3 for a constant value of $\tilde{D}_r$. We interpret this as $\tilde{D}_r$ changing as a function of orientation and apply eq 3 to evaluate $\tilde{D}_r$. Figure 7 shows $\tilde{D}_r$ as a function of strain rate and Figure 8 plots $\tilde{D}_r$ as a function of retardation (orientation) in the center of the mill. $\tilde{D}_r$ is clearly an increasing function of orientation, indicating the reduced molecular interactions in an oriented solution. This qualitatively supports the predictions of the Doi–Edwards theory.[11-13]

4.2. Nip Region (Method II). An effect that has been noticed during experimental observations that we judge is of considerable importance relates to changes in the character of the orientation in the nip region of the mill, that is as the solution passes the line joining the centers of adjacent rollers.

When the nip region is viewed between crossed polars with the incorporation of a full-wave plate, the observed retardation colors change from addition ($B > \lambda$) to subtraction ($B < \lambda$) (or vice versa, depending upon the full-wave plate direction) when passing from outside the nip into the mill interior. Between these two birefringent regions there exists a narrow zone of true optical isotropy close to but slightly displaced from the precise nip position. Figure 9 shows a diagrammatic representation of the whole of the four-roll mill.

These observations mean that the direction of maximum polarizability rotates through 90° on passage through the nip, which must reflect a corresponding change in rod orientation. As can be readily assessed from the colors, the orientation is such as to correspond to a rod alignment

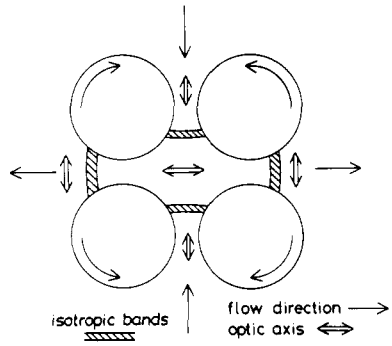

Figure 9. Schematic representation of the whole field of view in the four-roll mill. Single arrows show the flow direction and double arrows show the direction of the optic axis of the flowing PBT solution. The shaded areas represent the optically isotropic bands in the "nip" regions displaced inward between the inlet rollers and outward between the exit rollers, the magnitude of the displacement being exaggerated for the purpose of the sketch.

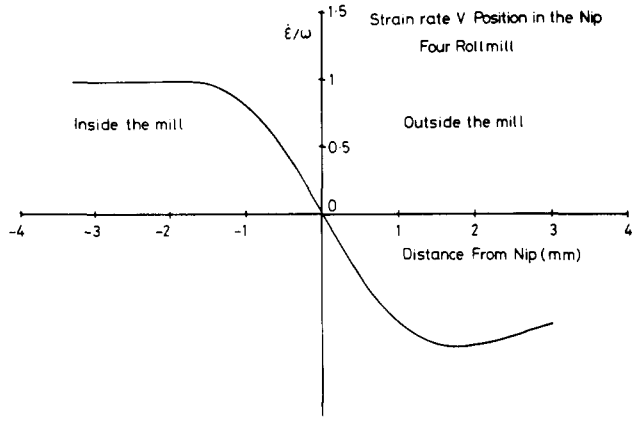

Figure 10. Calculated (strain rate)/(angular velocity) as a function of distance from the nip of the four-roll mill.

along the inflow direction outside the nip and along the outflow direction inside the nip, the latter already having been stated when describing the orientation within the mill interior.

Thus over a small localized region, the rigid molecules must "flip" from one orientation to the other in response to the changing flow field. Between the two areas of uniform orientation inside and outside the mill the molecular orientation is changing, passing through an isotropic region close to the precise nip position. It is readily visualized (Figure 9) that this flipover is the consequence of the changing nature of the flow, which will extend a given fluid element along the inflow and outflow directions outside and inside the nip (with relation to the roller), respectively. To our knowledge this observation is quite novel. It offers the possibility of exploring the response of the PBT molecule to a rapidly changing flow field and so determining its dynamic rotational diffusion and time constant parameters. As we shall see in ensuing sections this has consequences not only for PBT processing but to the theories describing the behavior of rigid macromolecules in solution.

4.2.1. Flow Field in the Nip Region. The flow field in the nip can be regarded as a pure extensional flow field that changes sign abruptly at the nip position. The corresponding shear rates have been calculated for the four-roll mill and the nature of the flow-field is illustrated in Figure 10 by plotting the shear rate normalized to the angular velocity of the rollers against distance from the nip along the inlet axis. (These precise values only apply to the present diameter of the rollers.) As can be seen the

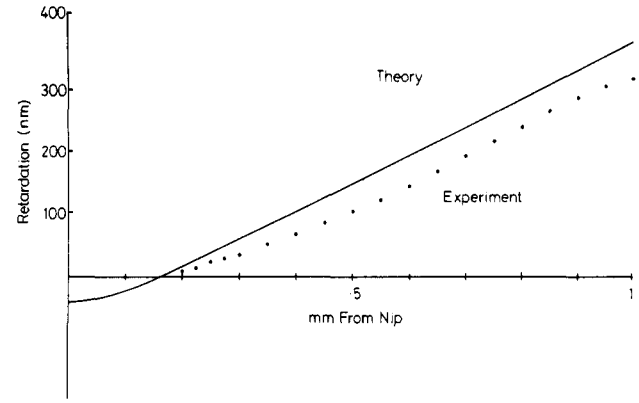

Figure 11. Retardation vs. distance from the nip: solid line, theoretical prediction; points, experimental results.

shear reverses sign on passing through the nip region and reaches a maximum.

It is actually observed that the isotropic dark band does not occur at the precise nip position but is displaced downstream by a distance that depends on shear rate and polymer concentration and is characteristic of the time constant of response of the molecules to the changing flow field. This displacement is incorporated in Figure 9, for sake of clarity, in a rather exaggerated form. There is a corresponding effect with the displacement in the opposite sense at the nip region along the outgoing axis arising from an analogous argument. The analysis to follow will be confined to the effect at the inlet region only.

Close to the nip position for the present dimensions of the mill (roller diameter 0.4 cm, separation 1 cm) we can approximate the extensional flow field as[23]

$$\frac{\dot{\epsilon}}{\omega} \approx \frac{0.04x}{f(0.5 - f)^2} \tag{4}$$

where $f = (R^2 - x^2)^{1/2}$ and x is the distance from the nip position (positive x downstream). For small x this reduces simply to $\dot{\epsilon}/\omega \approx 10x$.

The change in response of the retardation to the changing flow field is given at any instance by eq 1. The integration of this equation over the changing flow field of eq 4 is similar to the problem of creep responding to an applied stress history, giving

$$\frac{B(t)}{B_0} \simeq \frac{8\omega^2}{15\tilde{D}_r}\left[t + \frac{e^{-6\tilde{D}_r t} - 1}{6\tilde{D}_r}\right] + C \tag{5}$$

where C is a constant of integration equal to $-1/6\tilde{D}_r$ and the time delay to the isotropic state (t') is given by equating $B(t)$ to zero

$$t' + \frac{e^{-6\tilde{D}_r t'} - 1}{6\tilde{D}_r} = \frac{1}{6\tilde{D}_r}$$

To a good approximation this reduces to

$$t' = 1.85/6\tilde{D}_r \tag{6}$$

In the integration we have assumed $\tilde{D}_r$ constant, even though in reality we know that it is changing in response to the (small) change in shear rate over this region. We expect that the value of $\tilde{D}_r$ appropriate to the orientation at the nip position will dominate. D_r for the isotropic state is lower but the system is rapidly forced through this value by the now nonzero strain rate.

4.2.2. Retardation in the Nip Region. We are now able to measure the change in retardation as the solution responds to this well-defined flow field. Figure 11 shows

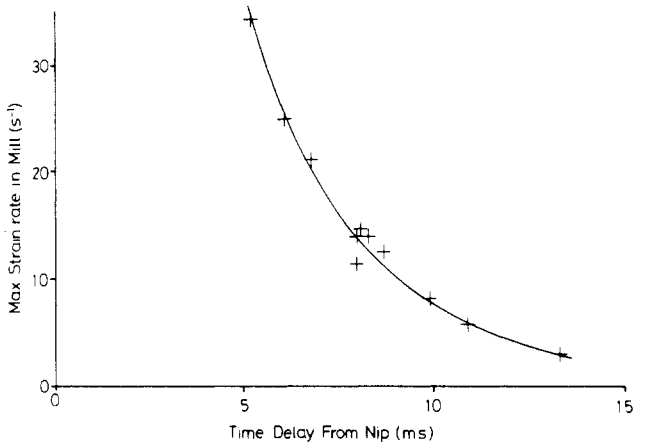

Figure 12. Maximum strain rate vs. time from nip to optical isotropy.

the measured retardation values as a function of distance dowstream (into the mill) from the precise nip position for a 0.5% solution. The isotropic state (zero retardation) is displaced by approximately 0.2 mm from the nip; from there on the retardation increases in response to the applied flow field. The solid line in Figure 11 shows the behavior predicted by the approximate theory above (eq 5), where $\tilde{D}_r$ has been fitted to give the correct position of the isotropic state according to eq 6 and time from the nip has been converted to distance, by the knowledge of the applied flow field (eq 4).

The value of B_0 used was that derived from measurement of birefringence of highly oriented thin films of solid PBT, corrected for solution concentration.

We can in effect quantity $\tilde{D}_r$ as a function of orientation by careful measurements of the time taken to achieve the isotropic state in response to the change in sign of the elongational flow field for a range of angular velocities of the rollers. Figure 12 shows a plot of the time lag of the isotropic band from the nip position for various maximum strain rates seen at that position. The time lag is a function of strain rate, and the predicted high strain rates give corresponding short time lags.

From eq 6 we know that the time constant of response should be $t' \approx 1.85/6\tilde{D}$, so we can calculate the rotational diffusion coefficient as a function of retardation at the nip. This is illustrated in Figure 8. $\tilde{D}_r$ is clearly increasing with retardation and hence with the orientation of the molecules, varying from ≈ 20 s^{-1} at zero retardation to 60 s^{-1} at 500-nm retardation. As for the equilibrium results for $\tilde{D}_r$ from the center of the mill, this is qualitatively in agreement with the Doi–Edwards theory, which predicts a progressive reduction in molecular interaction (increase in $\tilde{D}_r$) with increasing orientation.

4.3. Decay of Orientation on Cessation of Flow (Method III). A third and quite direct method of assessing $\tilde{D}_r$ is simply to observe the decay of retardation after the flow field is abruptly discontinued and observe the return to the unoriented state in the absence of external forces.

In this case B/B_0 decays as $e^{-6\tilde{D}_r t}$, so that a plot of ln (B/B_0) vs. time yields a gradient of $-6\tilde{D}_r$. In principle such a curve should provide a complete record of the process of disorientation; however, purely operational considerations restrict the range and accuracy of results based upon cessation of flow in the four-roll mill. For this reason the results have been supplemented with data from other experiments on sheared PBT solutions which enable the whole relaxation process to be monitored. That work will form the basis of a subsequent publication;[24] a few figures from that work will be included in the present paper for completeness.

5. Dependence of $\tilde{D}_r$ on Concentration and Orientation

5.1. 0.5% (w/w) Solution. All three methods (I), (II), and (III) above reveal that $\tilde{D}_r$ is an increasing function of strain rate, in qualitative agreement with the Doi–Edwards theory. With all three techniques we can obtain D_r for the isotropic state by extrapolations in a way appropriate to the three different methods of assessment. In the case of method I we extrapolate $\tilde{D}_r$ from curves such as Figure 7 to the zero strain rate or isotropic condition, in this instance yielding a value of $D_r \approx 15$ s^{-1}. Similarly, in the case of method II we extrapolate $\tilde{D}_r$ to the isotropic state from curves such as Figure 8, yielding $D_r \approx 20$ s^{-1}. Method III can yield much novel information about the decay processes, particularly from nearly perfect orientation;[24] for the present purpose however, we may obtain D_r simply by observing the decay of birefringence from very small levels of orientation toward the isotropic state.

Thus for the isotropic case, these three techniques are all available essentially simultaneously from the four-roll mill and yield consistent results, suggesting D_r values bounded by the region 1.6–20 s^{-1}. By all three methods this value increases toward 70 s^{-1} as the orientation is increased.

5.2. 0.025% (w/w) Solution. Again we have three techniques I, II, and III for estimating $\tilde{D}_r$. At the center of the mill (now because of the low concentration) the orientation is always much lower; hence the approximation to the isotropic state is even better. Over a range of strain rates the curves of B/B_0 vs. $\dot{\epsilon}$ were found linear and the value of $\tilde{D}_r$, using eq 3, is essentially constant at 150 s^{-1}. This constant value shows that although the orientation itself is still strongly dependent on shear rate, the molecular interactions are never significantly altered from those observed in the isotropic state. We can therefore take $\tilde{D}_r = D_r = 150$ s^{-1} (as obtained by method I), which accordingly should correspond to that appropriate to the totally unimpeded chain as expected in extreme dilutions (D_{r_0}; see below).

By method II utilizing the nip region, the orientations are again small, and so the estimation of τ_c, and hence $\tilde{D}_r$, is essentially that applicable to the isotropic state. We find $\tau_c \approx 1.2$ ms and hence $\tilde{D}_r = D_r \approx 140$ s^{-1}. This is in good agreement with the result found from birefringence measurements within the mill interior by method I above.

Cessation of flow in the four-roll mill (method III) cannot yield much information in this particular case since the time constants are so short. However, the decay process can be observed in the case of thin sheared PBT solutions,[24] yielding a value of $D_r \approx 160$ s^{-1}.

5.3. Higher Concentrations. At higher concentrations the molecular interactions have increased markedly, and this is reflected in the much lower values of $\tilde{D}_r$ obtained. From the center of the mill $\tilde{D}_r$ is again an increasing function of strain rate and orientation. By method I the extrapolated results for zero strain rate (D_r) are 0.4 and 2.2 s^{-1} at 1% and 0.75% concentrations, respectively.

Much larger displacements of the isotropic state from the nip position (method II) are observed. Again the results show a marked dependence on orientation, the zero-orientation values being 0.5 and 3.1 s^{-1} for concentrations of 1% and 0.75%, respectively.

In the case of concentrated solution the much lower $\tilde{D}_r$ values (longer time constants) enable an estimation of the value of D_r from the optical relaxation time (method III) when the flow in the mill is abruptly stopped. This value

Table I
Isotropic Rotational Diffusion Constant (D_r) (s^{-1})

concn, % w/w	from center of mill (method I)	from nip (method II)	from relaxation (method III)	Doi–Edwards	modified theory
0.025	150	140	160	0.08	$\sim D_{r_0}$ (160)
0.5	15	20	5	1.8×10^{-4}	1
0.75	2.2	3.1	1.2	0.9×10^{-4}	0.5
1.0	0.4	0.5	0.3	0.5×10^{-4}	0.3

is now in very good agreement with the results from the center of the mill and the nip region at $D_r \sim 0.3$ and 1–2 s^{-1} for 1% and 0.75% concentrations, respectively.

5.4. Summary of Results. In summary we have obtained values for $\tilde{D}_r$ as a function of strain rate and extrapolated to the isotropic state (D_r) by three techniques. First the measurements of retardation in the center of the mill, which gives $\tilde{D}_r$ for the equilibrium case, when flow-induced orientation and Brownian diffusion disorientation are equal. Second, the nip region gives a measure of the dynamic response of the solution, which is determined by the rate at which molecules can diffuse through each other to respond to the applied flow field. Third, measurement of relaxation of induced birefringence in the absence of elongational flow enables the diffusion processes alone to be observed.

Table I summarizes the results for isotropic D_r values for the four concentrations of solution. In what follows we shall consider these isotropic values for comparison with expectation from theory.

6. Doi–Edwards Theory

The Doi–Edwards model considers a test rod in solution surrounded by other rodlike molecules that contrain its rotational diffusion. The theory postulates that the test rod will only be released from its local constraints by the diffusion away of one of the constraining rods. Because the solution is quite strongly entangled, Doi and Edwards consider that rotational diffusion and lateral translational diffusion of the constraining rods are unlikely, leaving longitudinal diffusion (which is little affected by entanglements) as the dominant process for release of constraints. They consider that a constraint will be released when the rods have diffused a distance L along their lengths. This will be followed by an effectively instant rotational jump of the rod to a new location. The size of the jump is determined from the radius (a) of an imaginary cylinder surrounding the test rod that will be expected on average to contact one other rod. This is then interpreted as an angular jump a/L. This process, repeated in successive releases of constraints, yields a random walk of jump size a/L and with a jump frequency determined by the time scale of diffusion by a distance L along the molecular length. The overall result may be expressed as

$$D_r \approx D_{r_0}/c^2L^6 \tag{7}$$

where D_{r_0} is the unconstrained rotational diffusion coefficient (that applicable to infinite dilution), D_r is the predicted value, c is the number of rods per unit volume, and L is the length of the rod. No allowance is made in the theory for spatial constraints due to the diameter of the rod.

In order to apply this theory to our results we need two parameters: D_{r_0}, the unconstrained rotational diffusion coefficient, and L, the molecular length.

6.1. Value of D_{r_0}. There are a number of theories for the calculation of D_{r_0} due to Perrin,[25] Kirkwood and Auer,[26] Brenner,[27] and others. The relationships are similar and depend strongly on molecular length L, solvent viscosity η_s, and to a lesser extent molecular diameter d. The general form is $D_{r_0} = A[\ln (L/d)/\eta_s L^3]$, where A is a constant for a given temperature. The single most important parameter in this equation is the molecular length L. This can be ascertained from the measured intrinsic viscosity (η_0).

Following the formula of Kirkwood and Auer[26] and detailed by Bird[14]

$$[\eta_0] = \frac{4}{45}\frac{\pi N}{2M}\frac{L^3}{\ln (L/d)}$$

where N is Avogadro's number and M is molecular weight. In many complex systems (e.g., meromyosin) this has enabled the accurate prediction of $[\eta_0]$ (or conversely L) with no adjustable parameters.[14]

If we apply this relationship to the present case (intrinsic viscosity 32 dL/g), we predict L to be of the order of 210 nm for our particular PBT polymer sample. Undoubtedly the polymer is polydisperse (though we have learned subsequently that this polydispersity may be small), so one should be aware that the value for L is a weighted mean. Knowing L, we need only the values of the solvent viscosity and d to estimate D_{r_0}. We have measured the viscosity of the solvent as 16 cP and take d as $\approx$0.6 nm (though the dependence on d is slight). We thus predict from different treatments that D_{r_0} for intrinsic viscosity 32 dL/g PBT in methanesulfonic acid/chlorosulfonic acid should be as follows: Perrin, 156.9 s^{-1}; Kirkwood and Auer, 151.3 s^{-1}; Breenner, ellipsoid, 156.9 s^{-1}; Brenner, rod, 160.2 s^{-1}.

Note that the different theoretical treatments give closely corresponding results for D_{r_0}; we may say with some confidence that D_{r_0} is of the order of 160 s^{-1} for this polymer in methanesulfonic acid/chlorosulfonic acid solutions.

6.2. Comparison of Doi–Edwards Theory with Results. We can now compare the predictions of the Doi–Edwards theory for isotropic rotational diffusion coefficient with out experimental observations. Applying Doi and Edwards' relation for D_r to the 0.5% solution, we obtain $D_r = 1.47 \times 10^{-6} D_{r_0} = 1.7 \times 10^{-4}$ s^{-1}, which is less than the measured result ($\sim$20 s^{-1}) by a factor greater than 10^3.

For the 0.025% (w/w) solution the Doi–Edwards theory yields $D_r = 5.9 \times 10^{-4} D_{r_0}$ whereas experiment shows that D_r is significantly almost equal to D_{r_0}.

The 0.75% and 1% solutions are probably beyond the range of applicability for the Doi–Edwards theory; however, the values of D_r predicted are 0.9×10^{-4} and 0.5×10^{-4} s^{-1} compared with the experimentally observed values of 2 and 0.4 s^{-1}, respectively. The values of D_r predicted by the theory are summarized in Table I.

The values of D_r for PBT could be increased by aggregation of the molecules, which effectively increases the dimensions of the orienting objects while decreasing concentration in terms of number of rodlike objects per unit volume. Reported degrees of association[28] are of the order of 1.5 for a carefully prepared solution, which is not great enough to account for the discrepancy between observed and predicted values of D_r.

It seems in general that the Doi–Edwards theory seriously overestimates the degree of molecular interaction and

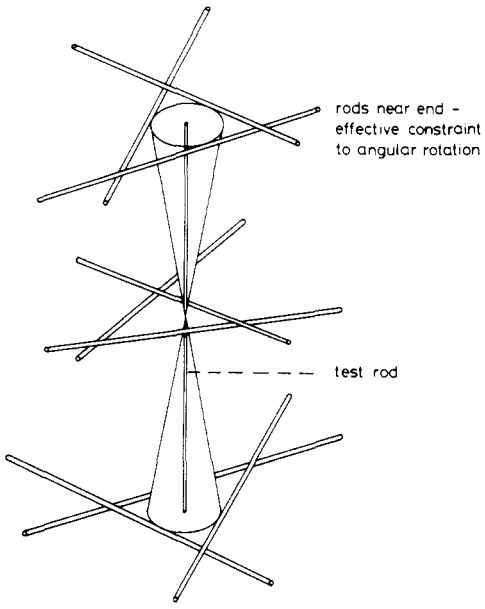

Figure 13. Environment of the test rod in the modified theory.

correspondingly underestimates the molecular mobility in this rodlike polymer solution. Thus the constraints in the theory must be far too severe.

The need to introduce a large numerical factor in the doi–Edwards expression has been observed previously.[1,29-31] Indeed recent Monte Carlo computer modeling of rigid-rod solutions has also shown the need for large correction factors.[32]

In what follows we shall attempt to resolve this problem along two lines. First we shall keep to the conceptual framework of the Doi–Edwards theory and shall attempt to reduce the mean constraints in their model. As we shall see there are good reasons for doing so, and in fact a reasonable fit between our data and theory can be achieved. Nevertheless as a further step we shall scrutinize the basic concept of a mean constraint theory. As will be seen its applicability to the present problem will appear seriously questionable as a result of it.

7. Reexamination of Doi–Edwards Theory: Relaxation of the Mean Constraints

The Doi–Edwards theory treats the test rod as stationary and awaits the diffusion away of constraining rods to determine the jump frequency. The converse case is to consider the constraining rods as essentially stationary and examine the diffusion through these rods of the test rod. The most effective entanglement constraints to rotation of the test rod about its center are confined to the end region of the rod, as illustrated in Figure 13.

Rods near the center of the test rod would need to be very much closer to prevent angular rotation. Suppose we say that the test rod is bound on average by four effective constraints which we expect to be, on average, in the last quarter section of the rod. In this case if the rods are positioned at random, we would expect one constraint to be released if the test rod diffused $L/16$ along its own length. Granted the test rod can expect to encounter a new constraint during this diffusion, but it is extremely improbable that the new constraint will be in such a position as to prevent the test rod jumping into the newly available space.

If the time taken to diffuse $L/16$ is τ_0

$$\tau_0 = L^2/256D_{t_0}$$

where D_{t_0} is the longitudinal translation diffusion coefficient. $D_{t_0} = {}^3/_2 D_{r_0} L^2$ (from basic diffusion theory[8]). Hence the jump frequency

$$\frac{1}{\tau_0} = \frac{256D_{r_0}(3L^2)}{2L^2} = 384D_{r_0} \tag{8}$$

By a similar argument the size of the angular jump should be based on consideration of the most *effective* constraints, which occur near the rod ends. Again using the chosen criterion, that we will consider constraints occurring at the last quarter sections of the rod, we can calculate a jump size of

$$a = 8/\pi cL^2$$

Thus we have (as Doi and Edwards) a random walk of step size a and jump frequency $1/\tau_0$, yielding an effective rotational diffusion constant of

$$D_r = 24576D_{r_0}/\pi^2 c^2 L^6 \tag{9}$$

For a 0.5% (w/w) solution this predicts $D_r \approx 1\ s^{-1}$, now in good agreement with the experimental result.

For the 0.025% (w/w) solution we predict $D_r = 200\ s^{-1}$. This is actually higher than D_{r_0} (150 s^{-1}). The approximation that jumps will occur essentially instantaneously once a constraint is released is only valid as long as $D_{r_0} \gg D_r$. Over a large range of applicability this would not seem to be the case, so that in these dilute solutions the value of D_r should be limited not only by the jump frequency and size but also by the finite time required to make the jump, so that D_r can clearly never exceed D_{r_0}. In close agreement with experiment we therefore expect D_r to be very close to D_{r_0} for 0.025% (w/w) solutions.

When the condition that $D_{r_0} \gg D_r$ is not satisfied, so the jumps can no longer be considered instantaneous, the predicted dependence of D_r upon the other parameters (especially molecular length, L) may be expected to break down. In particular, the power dependence of D_r upon L should be reduced from the predicted ninth power (eq 7, substituting for D_{r_0}).

The adjusted theory predicts that rotational diffusion is much closer to longitudinal translation diffusion values; this means that the initial assumption that translational diffusion is the only effective means of releasing constraints does not rigidly hold. The constraints can be released appreciably by the rotational diffusion of the constraining rods, a cooperative process that will yield yet higher values for the predicted D_r.

Even for the 1% solution the adjusted theory predicts D_r of 0.3 s^{-1}, which agrees very closely with the measured values (0.3–0.5 s^{-1}), even though the concentration should be too high to be treated by the Doi–Edwards theory. Over what range of concentrations can we expect such theories to hold, and how do the adjustments to the Doi–Edwards theory affect this?

Clear the first assumption by which the theory would break down is that of unrestricted diffusion of rods along their lengths. Indeed in the isotropic case it is relatively easy to calculate how far we expect a rod of a given diameter to diffuse along its length before it meets another rod, independently of the mechanism of diffusion.

The theories will break down when the distance of free diffusion becomes less than the mean expected diffusion distance needed to release one constraint, which is L in the Doi–Edwards theory and $L/16$ in the adjusted theory. The expected translational diffusion distance before end clash falls below $L/16$ for concentrations $\gtrsim$1.5%. Conversely, we can ask how much freedom does a rod need in order to get around such an obstacle when it is encoun-

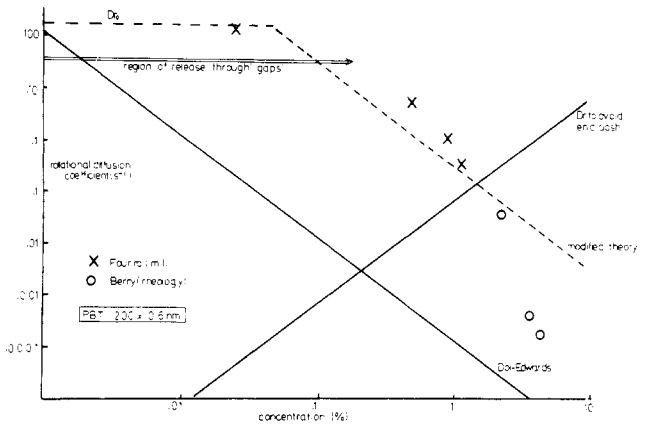

Figure 14. Log–log plot of D_r vs. concentration for Doi–Edwards theory, modified theory, and experiment.

tered; this clearly corresponds to an angular jump of the order of d/L. The calculated jump size falls below d/L for concentrations greater than ~1.5%.

We can define an *effective* rotational diffusion coefficient D_{r_e}, which is based upon the frequency of end clashes and the jump size needed to get around an end clash as a function of concentration. This corresponds to the minimum value of D_r at each concentration in order that the effects of end clashes should not dominate the process of diffusion. Figure 14 summarizes both experimental results and the theories and demonstrates the effect of restrictions on free diffusion along the length of the rod. The figure is plotted as log (D_r) vs. log (concentration) so that the theories reduce to straight-line plots. The solid line shows the prediction of the Doi–Edwards theory (eq 7) and the broken line shows that of the adjusted theory (eq 9). The horizontal broken line shows the limiting value of D_{r_0}, the rotational diffusion coefficient for noninteracting rods.

The theories should be applicable up to that concentration beyond which the value D_{r_e} necessary to avoid end clashes exceeds the theoretical prediction for D_r: 0.2% concentration for the Doi–Edwards theory and 2.7% concentration for the adjusted theory. Beyond these concentrations we would expect end collisions to occur more frequently than release of constraints and that the size of available jump angles will be too small to get around an obstacle when it is encountered, thus giving rise to a dramatic decrease in molecular mobility.

The measurements from the four-roll mill lie close to the modified theory up to 1%, the highest concentration studied. Beyond this concentration, results are available for the rheological time constants of very similar PBT solutions at zero strain rate from the work of Chu et al.:[28] these are shown as circles in Figure 14. As can be seen above 2% concentration there is a dramatic decrease in molecular mobility, D_r decreasing by 2 orders of magnitude between 2 and 3%. All arguments of this type are based upon approximations and would be expected to yield at best the correct power dependence of D_r upon parameters and a rough estimate of numerical factors.

8. Computer Model of Diffusion of Rigid Rods: Indication of the Inadequacy of the Mean Constraint Approach

In order to gain a greater insight into the mechanism of diffusion of rigid rods a computer program has been developed that models this system. The computer first establishes a "solution" of randomly positioned rods 100 nm × 1 nm, ensuring by contact criteria that rods cannot overlap. The solutions tested have all been isotropic in

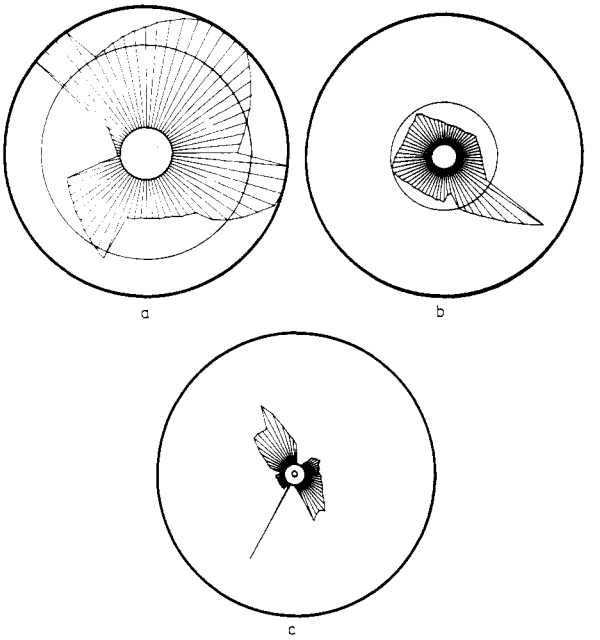

Figure 15. Polar diagram of the computer prediction of available disorientation angles for 100 1-nm rods at concentrations of (a) 0.01%, (b) 0.02%, and (c) 0.1%. The angular scale is linear, the origin represents 0°, and the outer circle represents 90° rotation. The innermost circle shows the jump size envisaged by the Doi–Edwards theory and the intermediate circle that from our modified constraints applied to the same theory.

the first instance, but this is not a necessary restriction. The model then simulates diffusion through this solution of another single rod, continuously exploring the space available around the test rod by tilting the rod in all directions until constraints are encountered according to our contact criteria. The rod is allowed to diffuse along its own length by set fractions of the rod length (usually $L/8$) and its new environment is explored. The model and contact criteria assume a finite diameter of 1 nm for the rods and that the constraining rods form a fixed network. For such a solution the Doi–Edwards regime applies over the concentration range 0.003–0.3% (w/w) (assuming the same mass per unit length as PBT).

In this way we can obtain polar diagrams of available disorientation angles at any instant in the rod diffusion. Figure 15a shows such a diagram for a 0.01% solution. The rod is initially normal to the paper (along the z axis) at the center of the circle; the curved boundaries represent the greatest angular inclination to the z axis that can occur in any given direction. The outer circle represents an available rotation of $\pi/2$ from z, that is free rotation on the time scale of the existing constraints. The smallest circle shows the jump size envisaged by the Doi–Edwards theory and the intermediate circle that from the modified theory. As can be seen the constraints operating upon the rod are extremely anisotropic; in some directions the rod can disorient unconstrained, while in others the constraints to rotation are severe.

Figure 15b shows a 0.02% solution and Figure 15c a 0.1% solution. While the average constraint is clearly increasing, the actual space that the rod can explore is still extremely anisotropic. Figure 16 shows how the space available to a rod for disorientational rotation changes as it diffuses along its own length for a concentration of 0.05%. Successive plots represent diffusion by $L/8$. As it diffuses constraints are lost and new constraints encountered, approximately at the rates envisaged by the modified Doi–Edwards theory. It is important though that a direction of relatively free rotation persists during this

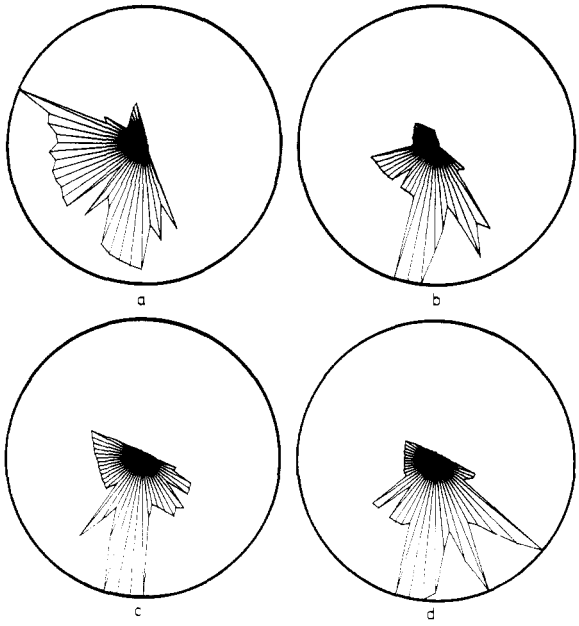

Figure 16. (a) As Figure 15 at 0.05% concentration. (b) Test rod diffused $L/8$ along its length. (c) Test rod diffused $L/4$ along its length. (d) Test rod diffused $3L/8$ along its legnth.

period of release of several constraints: diffusion into this "gap" is likely to dominate the disorientational process. Indicated in Figure 14 is the region of concentration over which we would expect diffusion into "gaps" to be the dominant process.

These diagrams clearly delineate the problems associated with the existing theories based upon mean values of jump frequency and jump size. First, at low concentrations the rods are unconstrained in some directions. In these cases it is more probable that a rod will diffuse unconstrained into one of these directions with a component of D_{r_0} rather than await the relatively infrequent release of a nearby constraint by longitudinal diffusion. This has significant consequences: the Doi–Edwards theory predicts an L^9 dependence on molecular length, through the agency of a random walk of jump frequency determined by D_{t_0}. If this is not the dominant process, but rotational diffusion is governed by a component of D_{r_0}, then the molecular length dependence will be closer to the L^3 dependence of D_{r_0}. Indeed Zero and Pecora have recently observed lower power dependencies of $\tilde{D}_r$ upon length for poly(γ-benzyl L-glutamate).[30] Second, at higher concentrations the probable distribution of disorientation angles will be an extremely uneven one for any chosen rod. Any theoretical treatment must incorporate this effect; taking merely a selected mean jump size and frequency is clearly inappropriate. It is necessary to consider the distributions of available disorientations.

In the course of our computer simulations we have been able to establish the form of these distributions by exploring many test rods and examining the frequency of occurrence of particular limiting angles of rotation. Figure 17a shows a histogram demonstrating the statistics gathered for a 0.01% solution. The frequency of limiting angles is quite constant, except for $\pi/2$ (free rotation) where there is a considerable peak, showing a large probability of

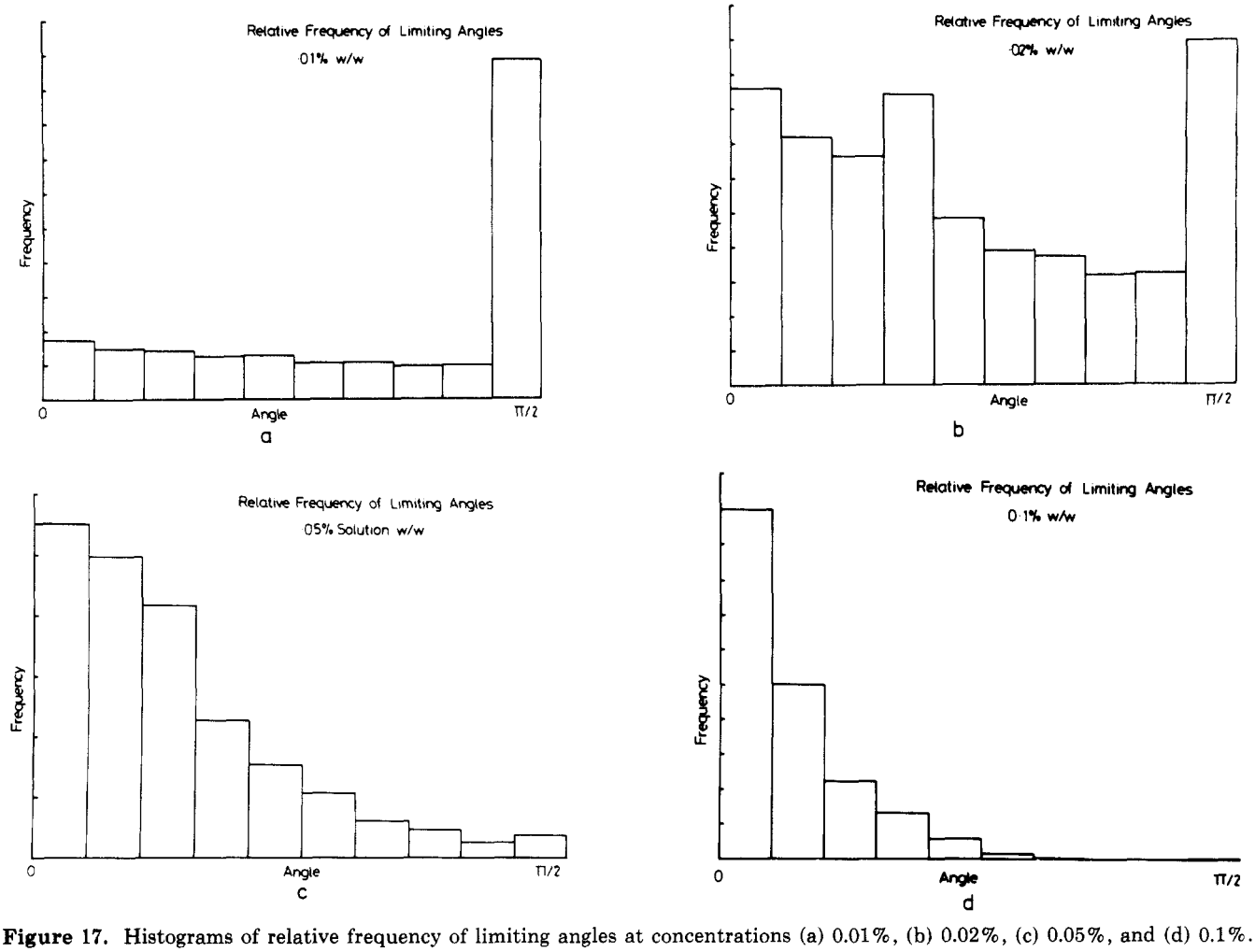

Figure 17. Histograms of relative frequency of limiting angles at concentrations (a) 0.01%, (b) 0.02%, (c) 0.05%, and (d) 0.1%.

relatively free rotation. Parts b–d of Figure 17 show similar histograms for 0.2, 0.5, and 0.1% concentrations, respectively. The probability of free rotations sharply reduces for increasing concentration, but the distribution curves still represent considerable unevenness.

While we have shown that the adjusted Doi–Edwards theory can account quite well for the experimental results in terms of concentration dependence (although over a higher concentration range than originally envisaged), the implication of the computer simulations is that the general method of diffusion (particularly at lower concentrations) will not be the release of constraints based upon a particular diffusion of rods lengthwise but that the rods will percolate into "windows" with a component of their uninhibited rotational diffusion coefficients (D_{r_0}). This is particularly important as D_r (and $\tilde{D}_r$) would not be expected to show the ninth-power dependence on molecular length as envisaged in the original theory, but some lower power tending toward the cubic dependence of D_{r_0}.

9. Conclusion

The orientability and diffusion of rigid rods in solution has been directly determined by registering the location and magnitude of the birefringence in a pure elongational flow field, as realized by a Taylor four-roll mill. The rotational diffusion coefficient ($\tilde{D}_r$) increases with orientation as envisaged by the Doi–Edwards theory, but absolute values are orders of magnitude greater than predicted; that is, the molecules are much less hindered than originally anticipated. The more detailed theoretical comparison is confined to the isotropic case (D_r). While a realistic modification was successfully applied to the existing theory, nevertheless computer simulations lead to a better physical insight into the process of diffusion and question the applicability of the existing theoretical approach relying on mean constraint.

At sufficiently long residence times in the flow field our results suggest that an initially isotropic solution may undergo a transition to a liquid-crystallike state. The technique has much potential for the study of such orientation-induced phase transitions.

Acknowledgment. We are indebted to Professor Sir Sam F. Edwards for helpful discussions, to the USAF Ordered Polymers Program for financial support and supply of material, and to SERC for support at the later stages.

Glossary of Terms

D_r	rotational diffusion coefficient of rigid-rodlike molecules in an entangled isotropic solution
$\tilde{D}_r$	rotational diffusion coefficient of rigid-rodlike molecules in a nonisotropic entangled solution (a function of overall orientation)
D_{r_0}	rotational diffusion coefficient of rigid-rodlike molecules in a dilute isotropic solution
D_{r_e}	minimum value of rotational diffusion coefficient required to avoid end clashes
D_{t_0}	longitudinal translational diffusion coefficient of a dilute solution of rigid-rodlike molecules
L	rod length
d	rod diameter
c	number of rods per unit volume
τ_c	orientational relaxation time
$\dot{\epsilon}$	strain rate
ρ	orientational distribution function
t	time
t'	time from the nip to the isotropic state
B	induced retardation
B_0	maximum retardation (perfect orientation)
ω	angular velocity of rollers
R	roller radius
h	half the separation of adjacent rollers
Δn	birefringence
x	distance downstream from the nip position
a	radius of an imaginary cylinder around a rod that touches only one other rod
$[\eta_0]$	intrinsic viscosity
N	Avogadro's number
M	molecular weight
λ	wavelength of light

Registry No. PBT (SRU), 69794-31-6.

References and Notes

(1) J. A. Odell, E. D. T. Atkins, and A. Keller, *J. Polym. Sci., Polym. Lett. Ed.*, **21**, 289 (1983).
(2) G. C. Berry, *Polym. Prepr., Am. Chem. Soc., Div. Polym. Chem.*, **18**, 146 (1977).
(3) G. C. Berry, "Contemporary Topics in Polymer Science", Vol. 2 E. M. Pearch and J. R. Schaefgen, Eds., Plenum Press, New York, 1977, pp 55–92.
(4) C. P. Wong and G. C. Berry, *Polymer*, *20*, 229 (1979).
(5) S. R. Allen, A. G. Filippov, R. G. Farris, E. L. Thomas, C. P. Wong, G. C. Berry, and E. C. Chenevey, *Macromolecules*, **14**, 1135 (1981).
(6) E. J. Roche, T. Takahashi, and E. L. Thomas, *ACS Symp. Ser.*, **No. 141** (1980).
(7) W. W. Adams, L. V. Azaroff, and N. K. Kulthreshana, *A. kristallogr.*, **150**, 321 (1980).
(8) S. R. Allen, A. G. Filippov, R. J. Farris, and E. L. Thomas, *J. Appl. Polym. Sci.*, **26**, 291 (1981).
(9) J. A. Odell, A. Keller, E. D. T. Atkins, and M. J. Miles, *J. Mater. Sci.*, **16**, 3309 (1981).
(10) C. P. Wong, H. Ohnuma, and G. C. Berry, *J. Polym. Sci., Polym. Symp.*, **No. 65**, 173 (1978).
(11) M. Doi, *J. Phys. (Paris)*, **36**, 607 (1975).
(12) M. Doi and S. F. Edwards, *J. Chem. Soc., Faraday Trans. 2*, **74**, 560 (1978).
(13) M. Doi and S. F. Edwards, *J. Chem. Soc., Faraday Trans. 2*, **74**, 919 (1978).
(14) R. Bird, O. Hasager, R. G. Armstrong, and C. F. Curtiss, "Dynamics of Polymer Liquids", Vol. II, Wiley, New York, 1977.
(15) D. P. Pope and A. Keller, *Colloid Polym. Sci.*, **255**, 633 (1977).
(16) M. R. Mackley and A. Keller, *Philos. Trans. R. Soc. (London)* **A278**, 29 (1975).
(17) M. J. Miles, K. Tanaka, and A. Keller, *Polymer*, **24**, 1081 (1983).
(18) G. I. Taylor, *Proc. R. Soc. (London)*, **146**, 501 (1934).
(19) M. R. Mackley, *J. Non-Newtonian Fluid Mech.*, **4**, 111 (1978).
(20) R. B. Bird, H. R. Warner, and D. C. Evans, *Adv. Polym. Sci.*, **8**, 1 (1971).
(21) M. Berry (Bristol), private communication.
(22) A. Peterlin, *J. Phys. Chem.*, **84**, 1650 (1980).
(23) S. J. Torza, *J. Polym. Sci., Polym. Phys. Ed.*, **13**, 43 (1975).
(24) J. A. Odell, to be published.
(25) F. J. Perrin, *J. Phys. Adium*, **5**, 497 (1934).
(26) J. G. Kirkwood and P. L. Auer, *J. Chem. Phys.*, **19**, 281 (1951).
(27) H. Brenner, *Chem. Eng. Sci.*, **27**, 1069 (1972).
(28) S. G. Chu, S. Venkatraman, G. C. Berry, and Y. Einaga, *Macromolecules*, **14**, 939 (1981).
(29) S. Jain and C. Cohen, *Macromolecules*, **14**, 759 (1981).
(30) K. Zero and R. Pecora, *Macromolecules* **15**, 87 (1982).
(31) Y. Mori and R. Hayakawa, *Poly. Prepr., Jpn.*, **32**, 694 (1983).
(32) M. Doi, I. Yamamoto, and F. Karo, *J. Phys. Soc. Jpn.*, **53**, 3000 (1984).